

Flow-plant interactions at a leaf scale: effects of leaf shape, serration, roughness and flexural rigidity

Ismail Albayrak · Vladimir Nikora ·
Oliver Miler · Matthew O'Hare

Received: 17 May 2010 / Accepted: 23 June 2011 / Published online: 14 July 2011
© Springer Basel AG 2011

Abstract The effects of leaf shape, serration, roughness and flexural rigidity on drag force imposed by flowing water and its time variability were experimentally studied in an open-channel flume at seven leaf Reynolds numbers ranging from 5 to 35×10^3 . The study involved artificial leaves of the same surface area but with three shapes ('elliptic', 'rectangular' and 'pinnate'), three flexural rigidities, smooth-edge and saw-tooth-like serration, and three combinations of surface roughness (two-side rough, one-side rough/one-side smooth, and two-side smooth). Shape was the most important factor determining flow-leaf interactions, with flexural rigidity, serration and surface roughness affecting the magnitude but not the direction of the effect on drag control. The smooth-edge elliptic leaf had a better hydrodynamic shape as it experienced less drag force, with the rectangular leaf showing slightly less efficiency. The pinnate leaf experienced higher drag force than the other leaves due to its complex geometry. It is likely that flow separation from 12 leaflets of the pinnate leaf prevented leaf reconfiguration such as leaflets folding and/or streamlining. Flexural rigidity strongly influenced the leaf reconfiguration and augmented the serration effect since very rigid leaves showed a strong effect of serration. Furthermore, serration changed the turbulence pattern around the leaves by

increasing the turbulence intensity. Surface roughness was observed to enhance the drag force acting on the leaf at high Reynolds numbers. The results also suggest that there are two distinctly different flow-leaf interaction regimes: (I) regime of passive interaction at low turbulence levels when the drag statistics are completely controlled by the turbulence statistics, and (II) regime of active interaction at high turbulence levels when the effect of leaf properties on the drag statistics becomes comparable to the turbulence contribution.

Keywords Aquatic plants · Leaves · Drag force · Reconfiguration · Flexural rigidity · River flow

Introduction

Aquatic plants in rivers and lakes encounter drag forces imposed by flowing water at multiple scales such as patch mosaic, patch, plant, shoot, stem and leaf scales (Nikora 2010). The physical interactions occurring at these scales are not independent but interconnected and together determine the total drag force experienced by a plant in the flow. In general, the total drag can be considered as a superposition of viscous friction at the water-plant surface interface and form (pressure) drag often associated with flow separation. To avoid uprooting and to prevent damage under high flow loads, plants can reduce the total drag by minimizing the plant surface area (to minimise viscous drag) and/or streamlining in flow direction (to minimise form drag). To achieve these, plants can develop, through adaptation, different strategies such as dynamic and static reconfiguration of plant bodies occurring at multiple scales, from a leaf scale to the patch mosaic scale. For example, a possible form of static reconfiguration at a leaf scale is leaf folding that reduces surface area and thus viscous skin

I. Albayrak (✉) · V. Nikora
School of Engineering, Fraser Noble Building,
University of Aberdeen, Aberdeen AB24 3UE, UK
e-mail: ismail.albayrak@abdn.ac.uk

O. Miler
Abt. Limnologie von Flusseen, Leibniz-Institut
für Gewässerökologie und Binnenfischerei,
Müggelseedamm 301, 12587 Berlin, Deutschland

M. O'Hare
Centre for Ecology and Hydrology Edinburgh,
Bush Estate, Penicuik, Midlothian EH26 0QB, UK

friction. Leaves can also control the drag through dynamic interaction with the flow (e.g., fluttering) via interplay of leaf rigidity, shape and surface roughness (dynamic reconfiguration, e.g., Usherwood et al. 1997; Nikora 2010). Static and dynamic reconfiguration in response to increasing flow velocity often leads to deviation from a quadratic relationship between the drag and flow velocity, even at fairly high Reynolds numbers (e.g., Armanini et al. 2005; Vogel 1989, 1994, 2009, Sand-Jensen 2003; Statzner et al. 2006). Despite plant leaves playing an important role in drag control at larger scales of patches and patch mosaics (e.g., Järvelä 2002; Wilson et al. 2003), very little is known about the physical mechanisms involved (de Langre 2008; Ennos 1999; O'Hare et al. 2010; Sand-Jensen 2003; Schouveiler et al. 2006; Vogel 1989, 2009).

Plants living either in still water or flowing water can be broadly categorized based on their habitat preferences (e.g., Riemer 1993; Ennos and Sheffield 2000): floating-leaved, emerged, submerged and free-floating plants. These plant types exhibit distinctly different leaf properties. The very thin cuticle on the leaves of submerged plants and on the lower leaf sides of floating-leaved and free-floating plants leads to a much smoother surface structure than found on the leaves of emerged plants and the upper surfaces of floating-leaved and free-floating plants. Furthermore, folding of the cuticle also contributes to roughness of the leaf surface (Koch et al. 2009). Employing definitions of hydraulically-smooth (roughness elements are submerged into a viscous sublayer) and hydraulically-rough (roughness elements protrude above the viscous sublayer) surfaces, we can distinguish, in general, three combinations: two-side smooth leaves; one-side smooth/one-side rough leaves; and two-side rough leaves. The rigidity of leaves also differs strongly between plant types. The leaves of submerged plants are thinner than the leaves of species that are exposed to the air with one or two sides. Hence, we expect them to be more flexible than the leaves of emerged, floating-leaved and free-floating plants. Leaf shapes vary and can also be characteristic of the plant type: floating-leaved species often have oval, round or strap-like shaped leaves with large surface areas to increase photosynthetic production (e.g., *Potamogeton natans* and *Glyceria fluitans*; Preston and Croft 2001). On the other hand, submerged species in rivers and lakes often have filamentous or finely diverged pinnate leaves. Typical representatives are species of the genus *Ranunculus* and *Myriophyllum*. Although leaf margins are generally smooth, some macrophyte species have finely serrated leaves, for example *Potamogeton crispus* and *Hydrilla verticillata*, which occur mainly in still water habitats or in slow flowing streams. The function of leaf serration has not been studied yet in detail for freshwater macrophytes, although its effect can be significant. Indeed, Chen et al. (1988) experimentally studied the effect of

irregularities (e.g., serration and transverse ridges) in the leaf surface on heat transfer and found that the irregularities disturbed the boundary layer on the plates (leaf models) and greatly increased heat transfer when the plate was parallel to the flow. In addition, Schuepp (1993) studied the effect of leaf morphology on leaf boundary layer for leaf models and leaves of terrestrial species. He reported that leaf shape, serration and roughness strongly influence the leaf boundary layer thickness and wake turbulence, and hence play an important role in plant-atmosphere interactions such as diffusion and transpiration at leaf surface. Similar effects can also be significant for aquatic leaves.

Overall, previous studies indicate that aquatic plant leaves have complex morphologies and biomechanical properties that evolved to accommodate specific features of their habitats, with leaf shape being probably the most important factor controlling plant performance (Tsukaya 2005). However, the nature and mechanisms of the interplay of leaf rigidity, shape, edges, and surface roughness are still largely unknown. Hence, the objectives of this study were (1) to experimentally investigate the individual and combined effects of leaf shape, serration, surface roughness, and flexural rigidity on the drag force statistics; (2) to identify effects of reconfiguration on drag control/reduction; and (3) to consider potential implications of leaf reconfiguration for the adaptation of macrophytes to different hydraulic habitats. In order to achieve these objectives, we completed a series of drag force and velocity measurements with artificial leaves of different shapes, serration, roughness and flexural rigidities.

Materials and methods

In this section, we describe the facilities and experimental setup, the measurement devices and the statistical parameters used in the associated data analysis, the materials (leaf characteristics), and the experimental procedure.

Facilities and experimental setup

Experiments were carried out in a glass-sided tilting flume with a flat bed in the Fluid Mechanics Laboratory of the University of Aberdeen. The flume is $B = 0.3$ m wide, $L = 12.5$ m long and $H = 0.45$ m deep (Fig. 1a). The experimental matrix included seven different flow rates with the constant water depth $h = 0.15$ m and bed slope 1:1,000 (Table 1). Since the depth and the bed slope were fixed, the hydraulic conditions deviated from the uniform flow regime. This deviation, however, was not critical for our study that focused on the local phenomenon of flow-leaf interactions. Measurements were carried out at a location 7 cm from the bed within the flume section 5–6 m from the flume entrance, where the flow field was fully

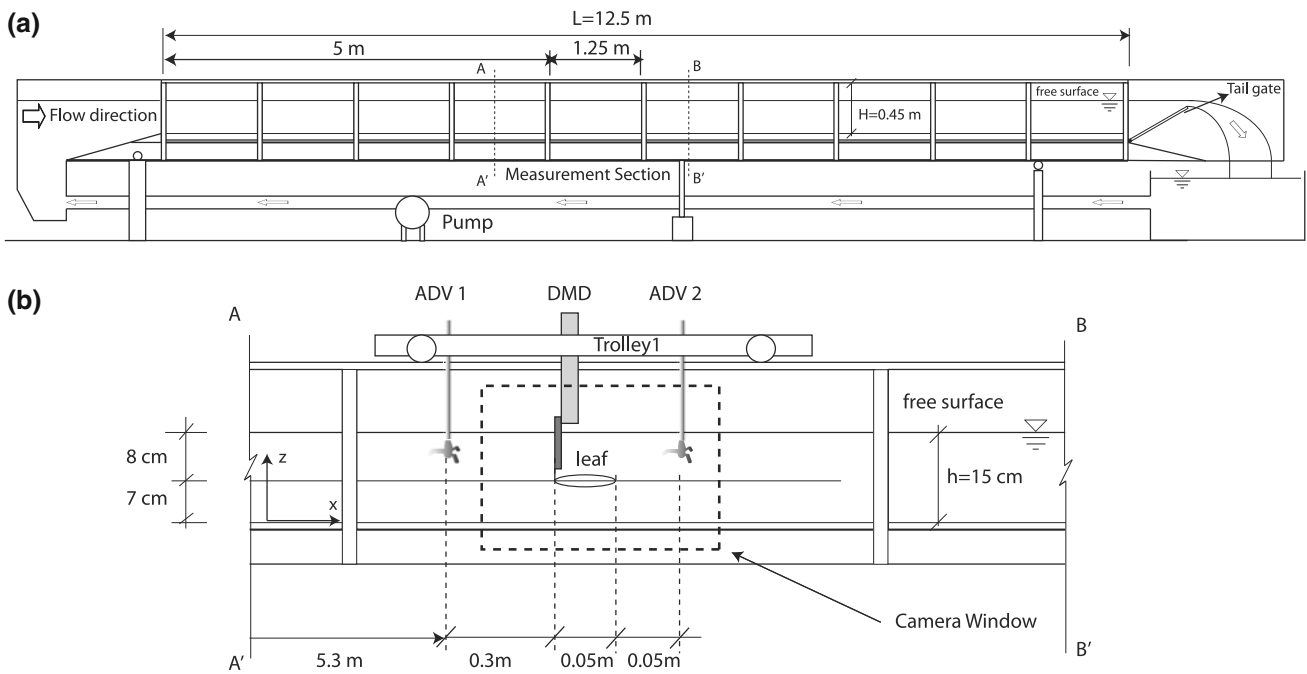


Fig. 1 **a** Schematic diagram of the glass-sided tilting flume set-up, and **b** a sketch of measurement section and position of ADV, DMD and Camera

Table 1 Hydraulic parameters for the experiments: h , water depth, Q , discharge, U_a , depth-averaged velocity, Re , leaf Reynolds number, Re_h , depth Reynolds number

h (m)	Q (m ³ /s)	U_a (m/s)	Re	Re_h
0.15	0.009	0.20	8.02×10^3	30.07×10^3
0.15	0.014	0.30	12.09×10^3	45.33×10^3
0.15	0.018	0.40	16.00×10^3	60.00×10^3
0.15	0.022	0.50	19.90×10^3	74.63×10^3
0.15	0.027	0.60	23.91×10^3	89.66×10^3
0.15	0.032	0.70	28.09×10^3	105.33×10^3
0.15	0.036	0.80	31.87×10^3	119.51×10^3

developed with a nearly homogeneous vertical profile of the longitudinal velocity away from the bed (Fig. 2).

Table 1 presents hydraulic parameters for the experiments performed for each leaf type (see definitions and explanations in the following sub-sections). In Table 1, the ‘leaf’ Reynolds number (Re) and ‘depth’ Reynolds number (Re_h) are computed as follows:

$$Re = U_a \sqrt{S} / \nu \tag{1}$$

$$Re_h = U_a h / \nu \tag{2}$$

where U_a and U_d are approach local (at a leaf level) and depth-averaged velocities, respectively, S is the (one-side) surface area of a leaf (equal to 0.0016 m²), h is the water depth, and ν is kinematic viscosity.

Measurement devices and associated data analyses

Drag measurement device

The drag measurement device (DMD) for this study was especially developed by the authors to measure drag force on a leaf and/or shoot (Fig. 3a). The DMD shown in Fig. 3a consists of a load cell, an elliptic shaped brass tube and a 10 cm high, 2 mm wide and 0.2 mm thick stainless steel rod. The rod is attached to the load cell as an extension of the beam and placed vertically in the center of the brass tube. A leaf can be easily attached to the tip of the rod by using super-glue. Any force applied to the rod and an associated leaf along the flow direction (Fig. 3a) results in deflection of the rod and the beam, leading to imbalance of the full Wheatstone bridge and generation of an output signal. The raw output signal was converted to the forces by using the equation obtained from the calibration of the device. The DMD allows measuring micro-scale forces (mN) with high accuracy at a sampling frequency from 1 to 1,000 Hz.

Calibration of the DMD was achieved by applying a series of known forces from 0.01 to 25 mN to the beam tip with the output signal being recorded by the Vishay 6100 data acquisition system at 50 Hz. The calibrations were routinely carried out before and after experiments. The relationship between the true input force and the output signal is shown in Fig. 4a. Non-linearity of the load cell (the maximum deviation of a calibration curve from a

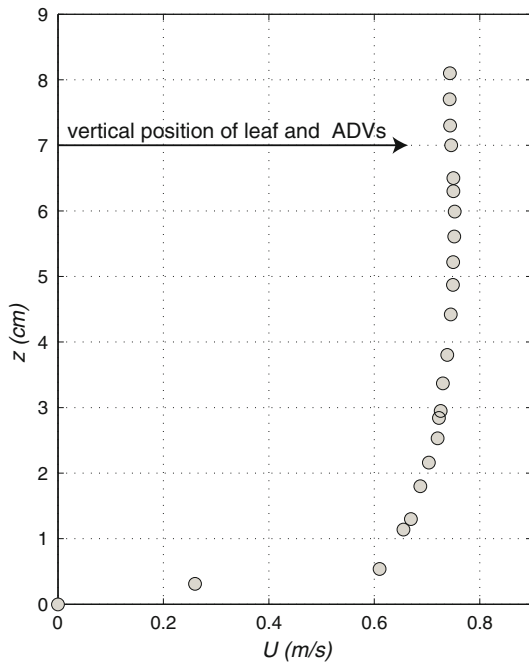


Fig. 2 An example of mean longitudinal velocity profile for $h = 15$ cm and $U_d = 0.75$ m/s

straight line drawn between the no-load and rated outputs) was specified as 0.05% of the rated load of 1 N by the load cell supplier. Non-linearity of the whole system based on the maximum load of 25 mN was 0.17%. Error in the load cell signal at no force was negligible and the electronic system was stable. Figure 4b shows the results of the tests carried out without leaf and with a rigid rough serrated

pinnate leaf (R5S2SK2, Table 3), and with a very flexible smooth elliptic leaf (R1S1FK0, Table 3). The measured drag force and its variance on the tip without a leaf did not exceed 10 and 7% of the total measured drag and its variance (i.e., tip + leaf), being around 2.5–5 and 0.5–4% in most cases, respectively. In the DMD data analysis, we subtracted the rod contribution from the total measured drag and its variance and calculated the standard deviation of the drag force from the net variance. Hence, only drag force acting on the leaves and its standard deviation were used in the interpretations.

The mean drag force on a leaf (F) was computed as:

$$F = F_m - F_t, F_m = \frac{1}{n} \sum_{i=1}^n F_{mi} \text{ and } F_t = \frac{1}{n} \sum_{i=1}^n F_{ti} \quad (3)$$

where F_m is the total time-averaged mean drag force (i.e., tip + leaf), F_t is the time-averaged drag force on the tip and n is the length of measured drag force time series (i.e., number of recorded data points for each experiment).

The measured instantaneous flow-induced drag forces were used to obtain bulk statistical characteristics such as mean, standard deviation, coefficient of variation, skewness and kurtosis. The standard deviation (σ_d) of the instantaneous drag force is a measure of its absolute deviations from the mean drag force; it was calculated using:

$$\sigma_d = \sqrt{\sigma_m^2 - \sigma_t^2}, \sigma_m^2 = \frac{1}{n} \sum_{i=1}^n (\hat{F}_{mi} - F_m)^2 \text{ and } \sigma_t^2 = \frac{1}{n} \sum_{i=1}^n (\hat{F}_{ti} - F_t)^2 \quad (4)$$

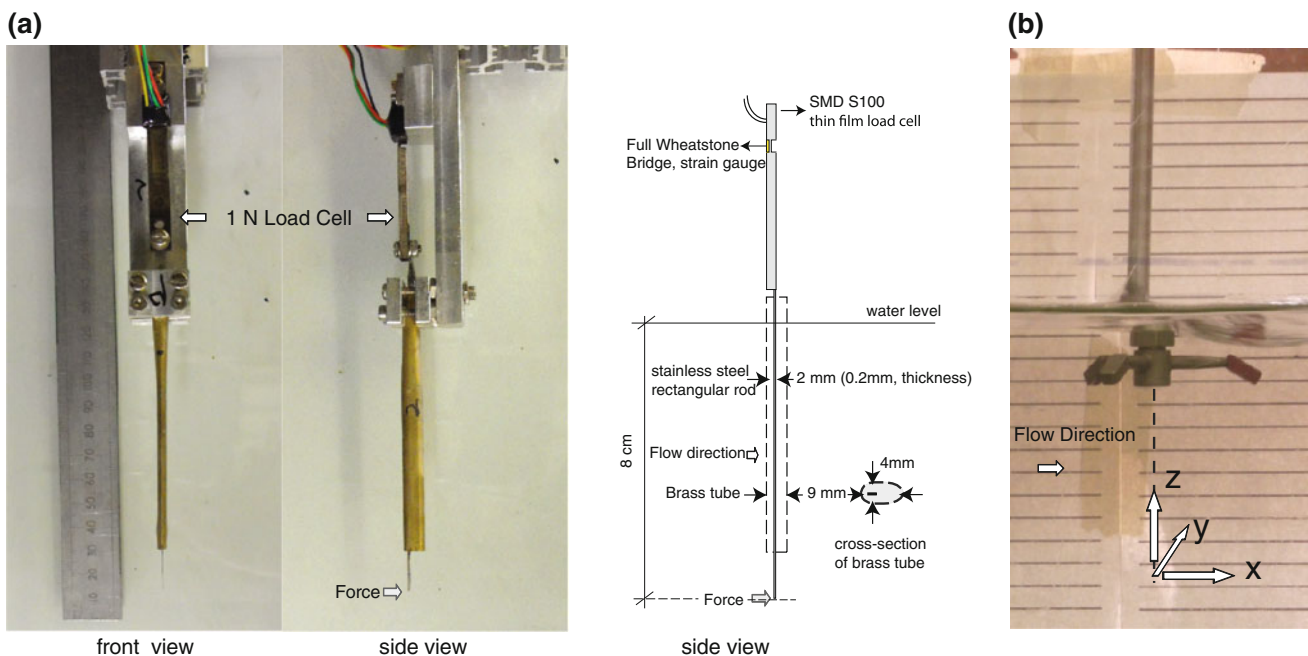


Fig. 3 a Drag measurement device (DMD), and b Acoustic doppler velocimeter (ADV)

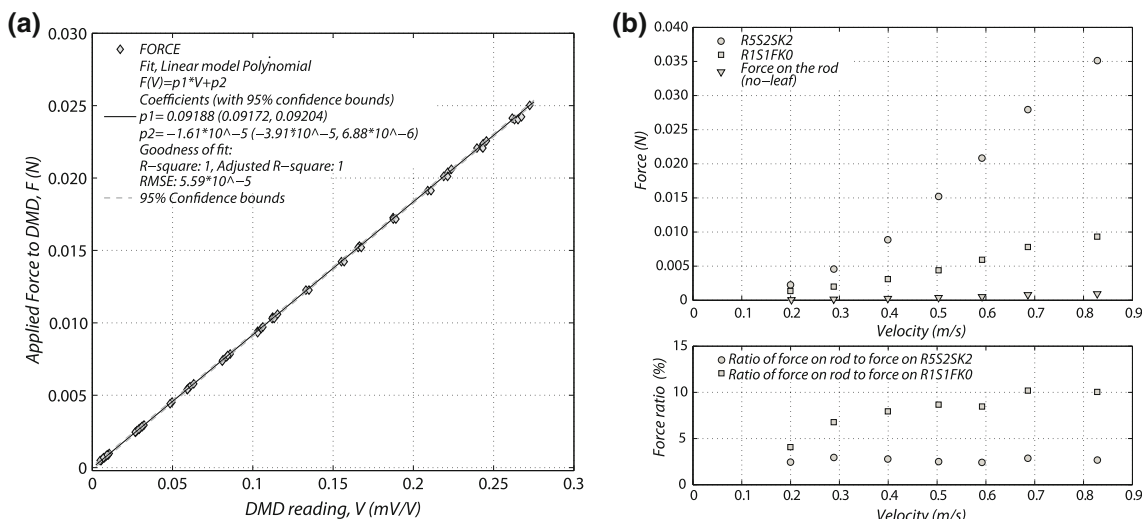


Fig. 4 **a** Examples of a calibration curve of the DMD, and **b** drag force measurements with and without a leaf (mean force versus mean flow velocity is shown)

where σ_m^2 and σ_t^2 are the total variance and the variance on the tip and \hat{F}_m and \hat{F}_t are the instantaneous total drag force and the instantaneous drag force on the tip, respectively. In our analysis, we also used a standard deviation normalized on the mean drag force, known as the coefficient of variation (CV), which is a measure of relative deviations of instantaneous drag force from its mean value:

$$CV = \sigma_d / F \tag{5}$$

CV complements σ_d and allows more meaningful comparisons between leaves of different shapes, rigidities, and other parameters. The mean, standard deviation and CV represent bulk statistics most commonly used to describe the statistical distribution of a variable. This approach may be sufficient when the distribution of a variable can be assumed to be normal. However, some degree of asymmetry (skewness) and peakedness (kurtosis) can exist in the probability distributions, ignorance of which may lead to under/over estimation of key drag-depending mechanisms. For instance, biophysical processes sensitive to extremes of the drag forces, such as the uprooting of plants, are likely to be underestimated unless the asymmetry in the data distribution is considered. Thus, the skewness (S_d) and kurtosis (K_d) may help better define the shape of the distribution of the instantaneous drag force and thus provide the information about its intermittent behavior. S_d and K_d were calculated using Eqs. 6 and 7, respectively:

$$S_d = \left(\frac{1}{n} \sum_{i=1}^n (\hat{F}_{mi} - F_m)^3 \right) / \sigma_d^3 \tag{6}$$

$$K_d = \left(\frac{1}{n} \sum_{i=1}^n (\hat{F}_{mi} - F_m)^4 \right) / \sigma_d^4 - 3 \tag{7}$$

In our analysis, we also employed a drag force parameterization as:

$$F = 1/2 \rho A_w C_d U_a^2 \tag{8}$$

where A_w is the leaf wetted area, and U_a is the time averaged velocity measured in front of a leaf, ρ is fluid density, and C_d is the drag coefficient, i.e.,

$$C_d = 2F / (\rho A_w U_a^2) \tag{9}$$

For rigid objects, the drag coefficient typically decreases with increasing Re (at small Re) and then attains a constant value at high Re (this region of independence of Re is known as a self-similarity region). For aquatic plants, however, C_d is not constant even at high Reynolds numbers and continues decreasing with increasing velocity, as a result of static and dynamic reconfiguration. Indeed, the deviation from a linear relation between the drag force and the squared reference velocity (expected from Eq. 8 for rigid objects at high Re) is likely associated with reconfiguration that leads to both the reduction of the reference area A and streamlining of a plant shape (i.e., reduction in C_d). Vogel (1989, 1994) expressed this combined effect of reconfiguration using an exponent α (known today as the Vogel number) that is a measure of deviation from expected behavior for rigid bodies, i.e., drag force $\sim U^{2+\alpha}$. If a leaf is rigid and Re is very high (so we can assume that $C_d = \text{const}$), its drag force is a function of U^2 alone (i.e., $\alpha = 0$). For a flexible leaf, one can expect $\alpha < 0$ due to leaf reconfiguration that modifies (reduces) both the drag coefficient and a representative area (Vogel 1989). Experiments show that individual freshwater plants often exhibit $\alpha \approx -1$ (e.g., Sand-Jensen 2003), while information for plant leaves is unavailable yet. The measured drag forces are used in this paper to assess this effect.

Acoustic doppler velocimeters

Velocity measurements were made using two Acoustic doppler velocimeters (ADV) at 7 cm above the flume bed (Figs. 1b, 3b). The upstream ADV was placed 30 cm away from the submerged tube of the DMD (Figs. 1b, 3a) in order to measure the undisturbed approach velocity and turbulence characteristics of the flow at a leaf level. The downstream ADV was placed 5 cm away from the back tip of a leaf to measure velocity and turbulence characteristics in the wake region of a leaf (Fig. 1b). Both ADVs were synchronized with DMD using an in-house-built electronic circuit. The ADVs and DMD were set to work at a sampling rate of 50 Hz as a standard set-up for each experimental scenario. The coordinate system is defined in Figs. 1b, 3b. For each run, the ADV performance was optimized for particular flow conditions by changing parameters such as velocity range and water temperature. ADV data were de-spiked using the phase-space thresholding method described in Goring and Nikora (2002). The streamwise fluctuating velocity (u'), used in this paper was obtained from the de-spiked instantaneous velocity time series as:

$$u' = u - U \quad (10)$$

where u denotes the instantaneous velocity, and U denotes the mean velocity in the x-direction (streamwise). The standard deviation (σ_{Ua}) skewness (S_{Ua}) and kurtosis (K_{Ua}) of the longitudinal approach velocity were calculated using equations similar to Eqs. 4, 6 and 7, respectively.

In addition, velocity spectra have been used to identify a noise floor and associated noise contribution to measured velocity variances, which have been used to correct σ_{Ua} , and K_{Ua} as described in Nikora and Goring (1998).

Video recording

For the visualization of flow-leaf interactions, a DV camera with a frame size of 640×480 pixels (*Width x Height*) and a frame rate of 25 *fps* was used in all experiments to perform video recordings of a 40 cm by 30 cm area shown in Fig. 1b. Video data were analyzed to obtain qualitative information on leaf motions at different flow velocities and on leaf reconfiguration.

Materials

Leaf characteristics

Natural leaves show high variation in their morphology and biomechanical properties, which remain poorly understood,

and thus the results of studies of natural leaves are difficult to generalize. For this reason, we simulated three basic leaf shapes (elliptic, pinnate and rectangular), and studied artificial leaves of these shapes under controlled conditions (Fig. 5). The one-side leaf surface area across shapes was kept constant and was equal to 0.0016 m^2 . Elliptic, pinnate and rectangular shapes were coded as S1, S2 and S3, respectively. In order to examine the effect of flexural rigidity of a leaf on drag force, leaves were made of plastic materials with different values of Young's modulus and thickness. Young's modulus, second moment of area and flexural rigidity (their product) of 6 mm wide representative strips of plastic materials used in our study are shown in Table 2. The details of tests of the materials can be found in Miler et al. (2011). Based on the material properties and leaf geometry, flexible, moderately rigid and highly rigid leaves were coded as R1, R3 and R5, respectively.

In nature, aquatic plants have leaves with edge shapes that vary in size from microns to millimeters, and thus it is important to investigate the leaf serration effect on drag force. Therefore, we have included in our study non-serrated leaves coded 'F' and serrated leaves coded 'S' for all shapes and rigidities. While non-serrated leaves have smooth edges, the serrated leaves have forward pointing teeth. A detailed sketch of the serration applied to the leaves is shown in the Fig. 5.

Finally, the roughness effect on drag force was examined by making the surface of artificial leaves rough. Roughness elements were made of 1.5 mm by 1.5 mm cut squares of the same plastic material as the leaf itself and glued on the surface in 4.75 mm by 4.75 mm grids as shown in Fig. 5. Two-side smooth, one-side smooth/one-side rough and two-side rough leaf experiments were coded as K0, K1 and K2, respectively.

Experimental procedure

For each of 54 leaf types (Table 3), velocity and drag force measurements as well as video recordings were carried out with synchronized ADVs, DMD and DV camera for 5 min at seven different flow rates (Table 1). First, a leaf was glued to the tip of the steel rod of the DMD and then the force measured by the DMD was set to zero in a still water tank where leaf was 8 cm below the water surface. Second, the DMD was positioned in the center of the flume between two ADVs as shown in Fig. 1b. The centers of the leaf and the ADVs' sampling volumes were at the same level positioned at 7 cm above the flume bed and at 8 cm below the water surface. The data collected from the ADVs, DMD and video camera were transferred to a high-speed computer for the post-processing and data analysis.

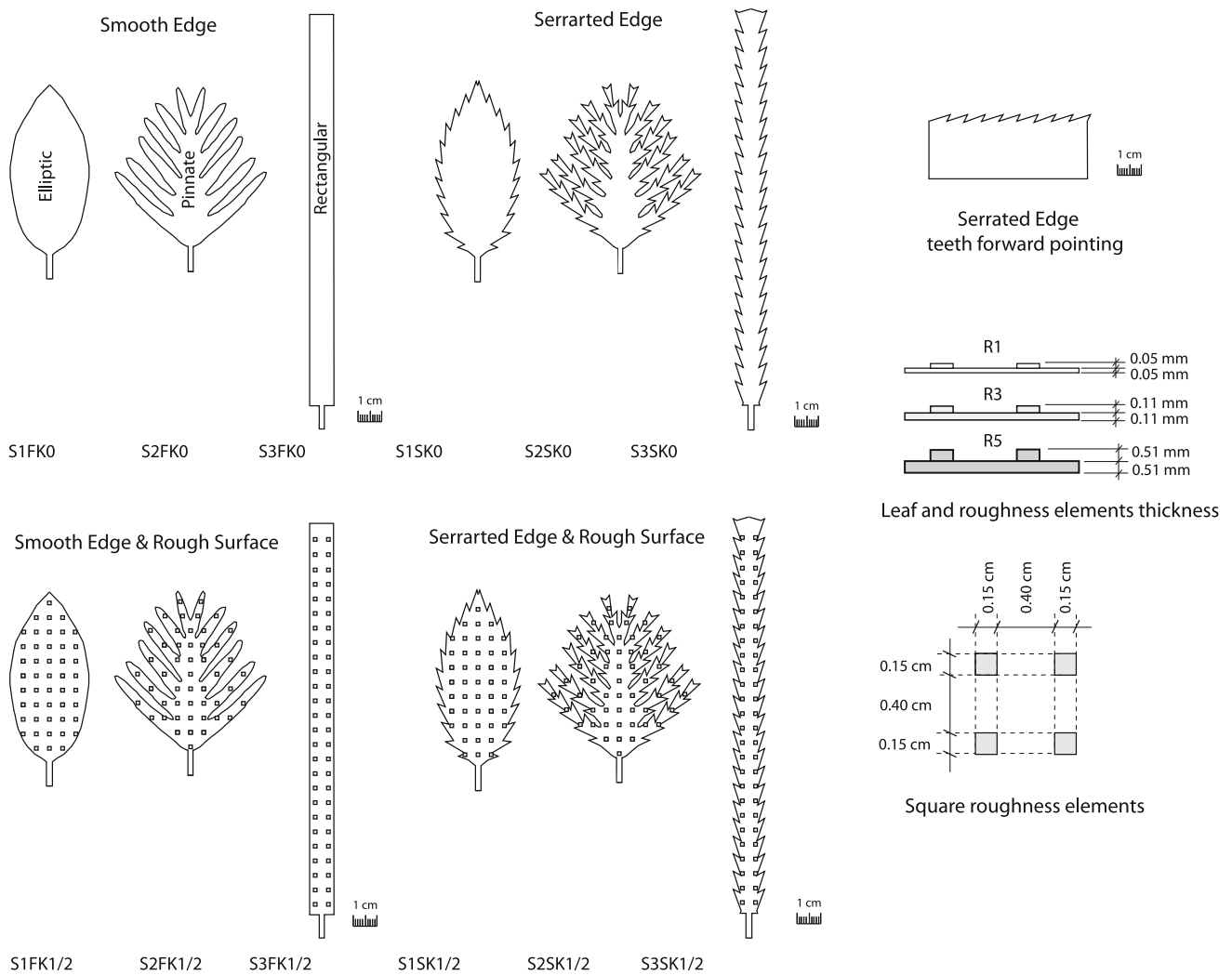


Fig. 5 Leaf characteristics: shape, serration and roughness

Table 2 Mechanical properties of the plastic materials used in the experiments

Experiment code	Thickness (mm)	Second moment of area I, (m ⁴)	Young's modulus (tension) E, (Nm ⁻²)	Flexural rigidity IE, (Nm ²)
R1	0.01	5×10^{-19}	300×10^8	1.5×10^{-8}
R3	0.06	1.1×10^{-16}	108×10^8	116×10^{-8}
R5	0.47	5.2×10^{-14}	13.6×10^8	7068×10^{-8}

Results

Effect of leaf shape

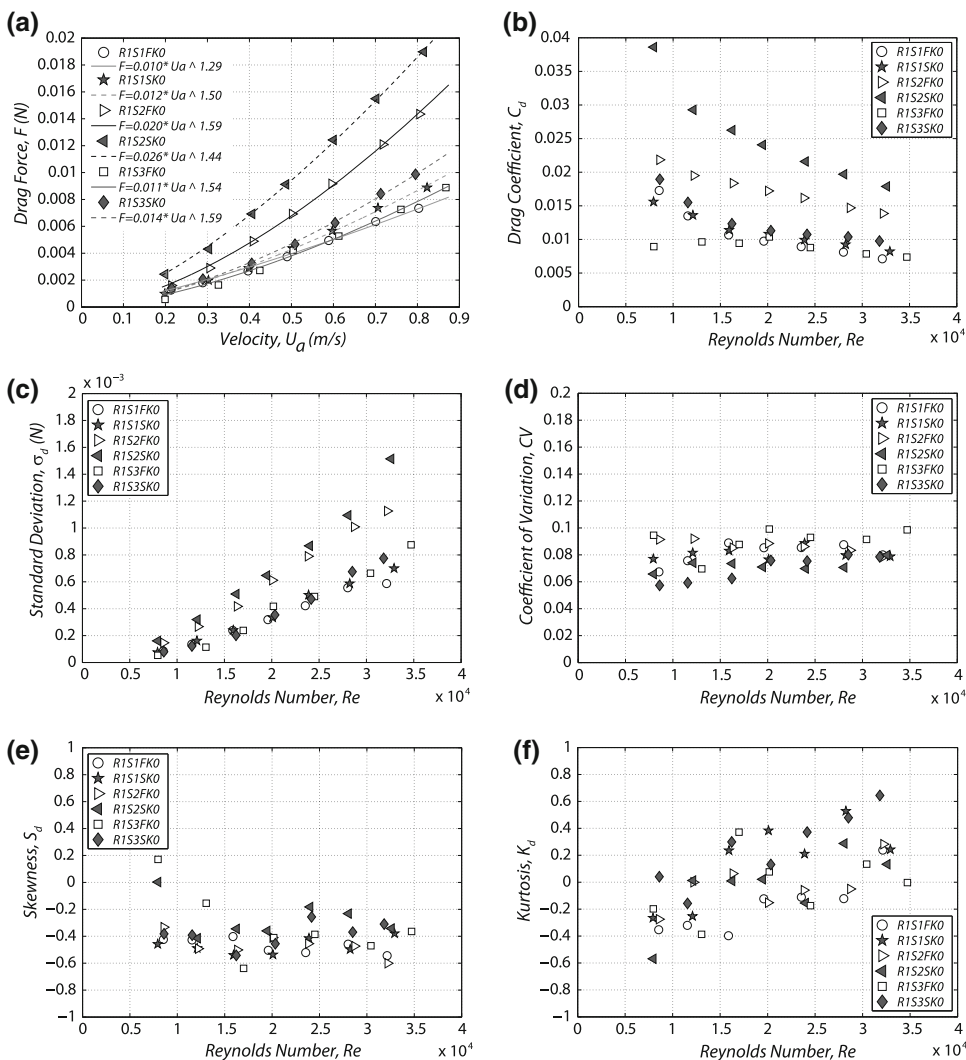
We first examine the effect of leaf shape on drag force for the elliptic, pinnate and rectangular shaped leaves with a smooth surface and smooth edges. In Figs. 6, 7 and 8 the time-averaged drag forces (F), its statistics and the drag coefficient (C_d) at three different flexural rigidities (R1, R3 and R5) are shown as a function of the mean approach velocity (U_a) and the Reynolds number (Re). The

experiments revealed a profound effect of shape on the drag force and drag coefficient. The drag force on the pinnate leaf is the largest at all studied velocities, significantly diverging from the drag force on the other two leaves as velocity increases, irrespective of leaf rigidity. In Fig. 6a, at lower velocities the drag on the rectangular leaf is slightly lower than the drag on the elliptic leaf, but as velocity increases, this trend reverses. This pattern changes with increasing rigidity (Figs. 7a, 8a), i.e., the drag forces on the elliptic and rectangular leaves are almost the same for R3, with higher drag acting on the rectangular leaf at

Table 3 Experimental matrix and codes of experiments

Rigidity	R1			R3			R5		
Shape	S1	S2	S3	S1	S2	S3	S1	S2	S3
Smooth edges	F			F			F		
Smooth	R1S1FK0	R1S2FK0	R1S3FK0	R3S1FK0	R3S2FK0	R3S3FK0	R5S1FK0	R5S2FK0	R5S3FK0
Rough 1	R1S1FK1	R1S2FK1	R1S3FK1	R3S1FK1	R3S2FK1	R3S3FK1	R5S1FK1	R5S2FK1	R5S3FK1
Rough 2	R1S1FK2	R1S2FK2	R1S3FK2	R3S1FK2	R3S2FK2	R3S3FK2	R5S1FK2	R5S2FK2	R5S3FK2
Serrated	S			S			S		
Smooth	R1S1SK0	R1S2SK0	R1S3SK0	R3S1SK0	R3S2SK0	R3S3SK0	R5S1SK0	R5S2SK0	R5S3SK0
Rough 1	R1S1SK1	R1S2SK1	R1S3SK1	R3S1SK1	R3S2SK1	R3S3SK1	R5S1SK1	R5S2SK1	R5S3SK1
Rough 2	R1S1SK2	R1S2SK2	R1S3SK2	R3S1SK2	R3S2SK2	R3S3SK2	R5S1SK2	R5S2SK2	R5S3SK2

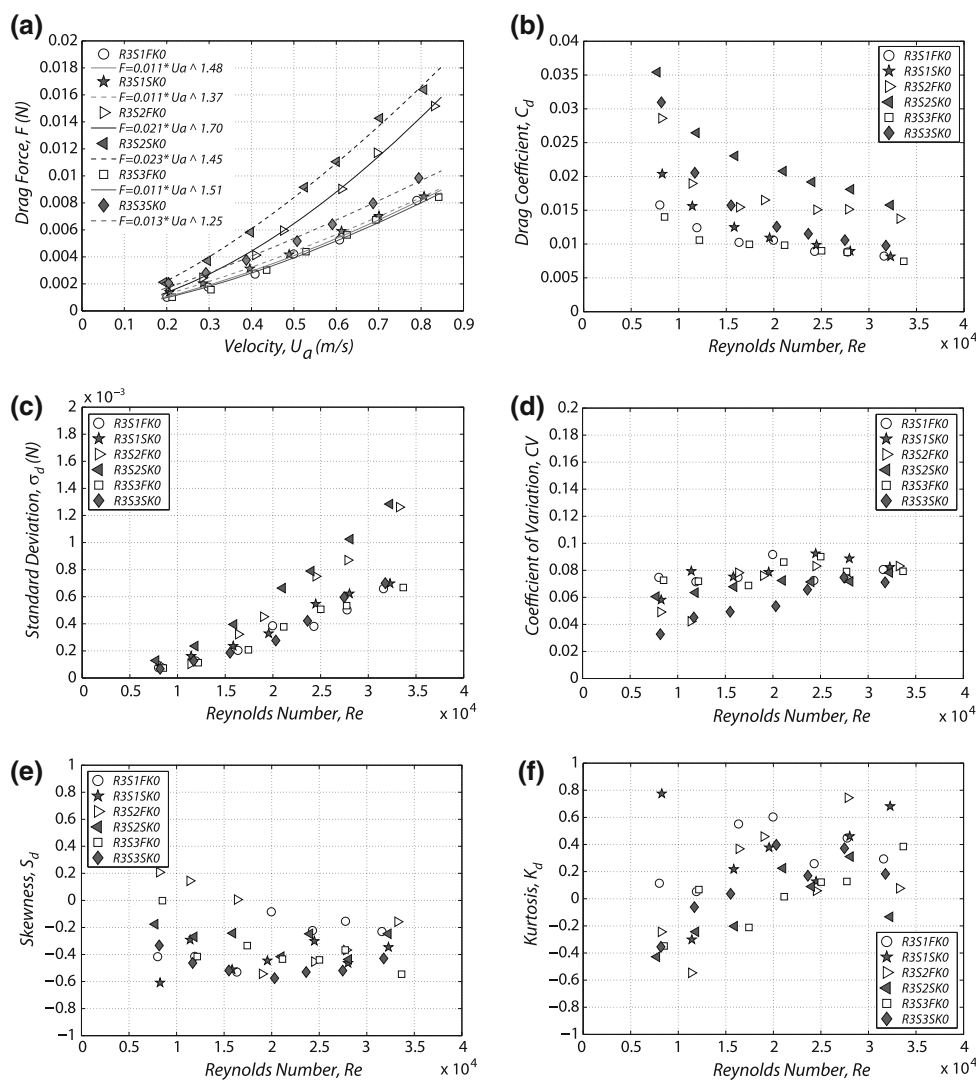
Fig. 6 **a** Plot of the drag force, F , versus the mean approach velocity, U_a , **b** Drag coefficient, C_d , **c** Standard deviation, σ_d , **d** Coefficient of variation, CV , **e** Skewness, S_d , and **f** Kurtosis, K_d of drag force versus Reynolds number, Re ; data for the smooth edged and serrated elliptic, pinnate and rectangular leaves of rigidity R1 are shown



R5. Figures 6, 7, and 8 also reveal significant effects of the leaf shape and rigidity on the drag coefficient. For all three rigidities, the curves $C_d = f(Re)$ show the highest C_d for the pinnate leaf and the lowest C_d for the elliptic and the rectangular leaves over the whole range of Reynolds

numbers, as one would expect. Another noticeable feature is that the rate of change of $C_d = f(Re)$ reduces with increase in leaf rigidity for all shapes, with its magnitude depending on the shape. One may note that C_d becomes nearly constant for the whole range of Re for the elliptic

Fig. 7 **a** Plot of the drag force, F , versus the mean approach velocity, U_a , **b** Drag coefficient, C_d , **c** Standard deviation, σ_d , **d** Coefficient of variation, CV , **e** Skewness, S_d , and **f** Kurtosis, K_d of drag force versus Reynolds number, Re ; data for the smooth edged and serrated elliptic, pinnate and rectangular leaves of rigidity R3 are shown



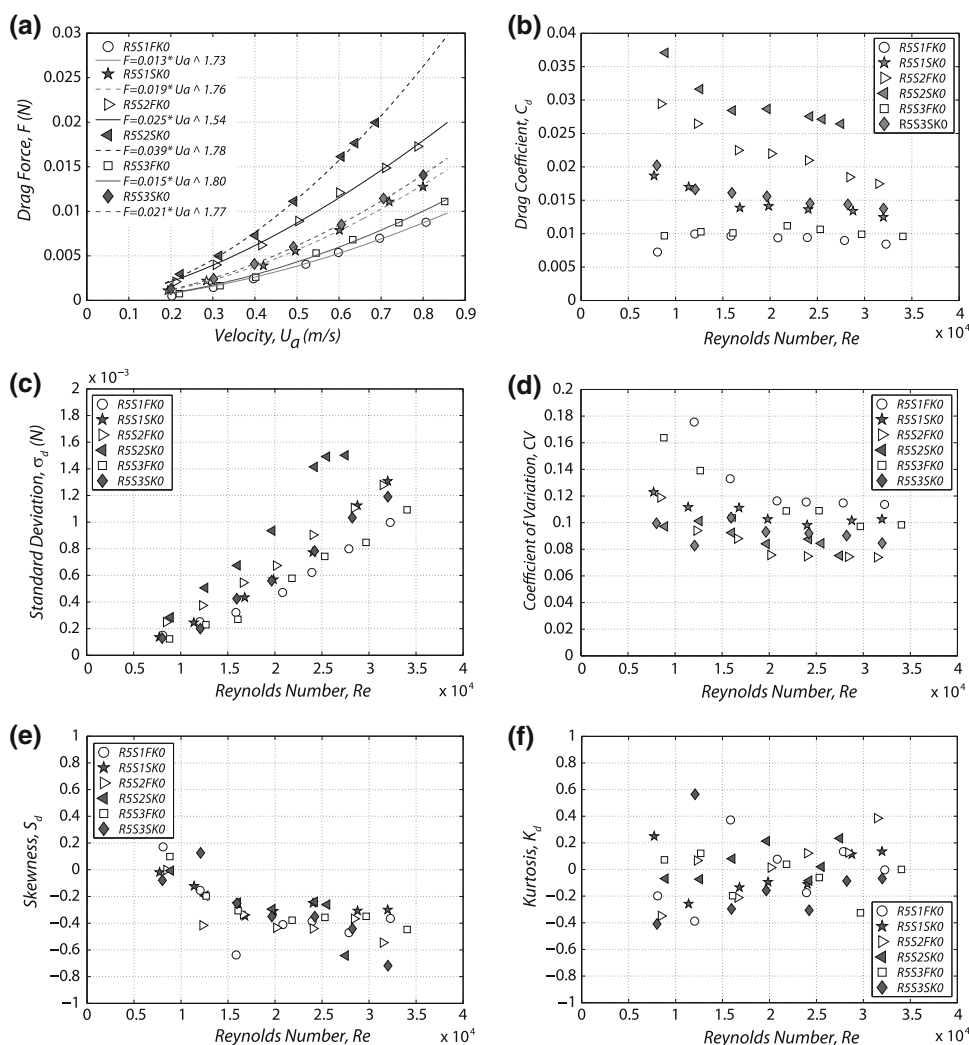
and rectangular smooth-edge leaves for R5 (Fig. 8b). Overall, depending on the leaf shape and rigidity, the drag coefficient varies within the range from 0.005 to 0.03 (Figs. 6b, 7b, 8b). The standard deviation of the instantaneous drag force increases with Re for all leaf shapes and rigidities (Figs. 6c, 7c, 8c). For the rigidities R1 and R3, the σ_d values for the elliptic and rectangular leaves nearly coincide for all studied Re , being 50% less than the σ_d of the pinnate leaf.

The corresponding values of CV slightly increase with Re at its smaller values becoming nearly constant at $Re > 15 \times 10^3$ (Figs. 6d, 7d, 8d). However, with further increase in rigidity (i.e., at R5), the patterns of σ_d and CV noticeably change: the magnitudes of σ_d and CV significantly increase while pattern of $CV = f(Re)$ reverses (i.e., instead of increasing as for R1 and R3, CV decreases becoming constant at $Re > 15 \dots 20 \times 10^3$). It is interesting that the CV of the pinnate leaf at R5 is much smaller compared to other leaves suggesting that due to its

complex geometry the shape contribution to the mean drag is higher than its contribution to the magnitude of drag fluctuations. The plots of skewness of the drag force (Figs. 6e, 7e, 8e) do not reveal any significant difference between the leaf shapes and rigidities, showing at the same time a tendency to decrease from positive 0.2 at the lowest studied Re to negative 0.4–0.5 at $Re > 15 \dots 20 \times 10^3$. The negative S_d indicates a long-left tailed distribution of drag forces, i.e. more frequent but smaller positive fluctuations and rare but deeper negative fluctuations. The plots of kurtosis K_d are similar for all shapes and rigidities demonstrating a tendency to increase from approximately -0.5 at lowest Re to 0.5 at highest Re , with change of K_d sign occurring at approximately $Re = 15 \times 10^3$ (Figs. 6f, 7f, 8f).

In summary, the elliptic leaf has the best hydrodynamic shape among the leaves as it experiences the least drag force, with the rectangular leaf performing slightly worse but still considerably better than the pinnate leaf. These

Fig. 8 **a** Plot of the drag force, F , versus the mean approach velocity, U_a , **b** Drag coefficient, C_d , **c** Standard deviation, σ_d , **d** Coefficient of variation, CV , **e** Skewness, S_d , and **f** Kurtosis, K_d of drag force versus Reynolds number, Re ; data for the smooth edged and serrated elliptic, pinnate and rectangular leaves of rigidity R5 are shown



highlighted findings show that the effect of leaf shape on drag force is strong and may further be enhanced by leaf serration and rigidity.

Effect of serration

As far as the elliptic and rectangular leaf shapes with high (R1) and moderate flexibilities (R3) are concerned, the serrated leaves experience on average 12% higher drag forces than the non-serrated leaves. The C_d s of the serrated leaves are slightly higher than the C_d of the non-serrated leaves and decrease rapidly at lower Reynolds numbers (Figs. 6b, 7b). With increasing rigidity (R5), the serration effect is much more profound, with a 40% increase in the drag force and the C_d (Fig. 8a, b). Interestingly, the effect of serration on the σ_d is negligible for the leaves with R1 and R3. Hence, a slight decrease in the CV of the serrated leaves is observed. However, at the highest rigidity, the serration strongly

affects the σ_d by increasing it at $Re > 20 \times 10^3$. On the other hand, the CV s of the serrated leaves decrease and become nearly constant at high Re numbers with being equal to 0.08 corresponding to the values for the non-serrated leaves. This result is surprising and indicates that at high Re , the serration effect on the CV is negligible and the magnitude of the drag fluctuations is not affected by the increasing ambient turbulence level independently of leaf shape.

A strong serration effect is observed for the pinnate leaf. Because of the serration, the perimeter of the pinnate leaf is increased and its geometry becomes more complex than for the other two leaves. This geometrical disadvantage is clearly seen in the relations between the drag force and C_d , and approach velocities and Reynolds numbers, respectively. The drag force increases, on average, by 34% for the serrated pinnate leaf with R1 and R3 compared to the non-serrated pinnate leaf, whereas at R5 it increases by 25%. The combined effects of rigidity, shape and serration on the

drag force, σ_d and C_d are maximized for the pinnate leaf with R5 which can be seen in Fig. 8a–c.

In comparison to non-serrated leaves, the serration effect on the S_d and K_d is not significant and this can be clearly seen from Figs. 6, 7 and 8e, f. Therefore, the shape of the probability distribution of the drag forces for the serrated leaves should be expected to be similar to those of the non-serrated leaves.

In general, for all leaf shapes, the serration of the leaf margins increases the leaf perimeter and modifies the geometry of the leaf, which likely causes disturbance and an early separation of the flow around the sawtooth-like serration of the leaf. The serration enhances the downstream turbulence intensity up to 5–10% over the approach turbulence intensity, obtained from the downstream ADVs velocity data. The magnitude of the serration effect on the drag force and the flow around the leaf depends on the rigidity and Re .

Effect of roughness on the performance of non-serrated leaves

For lower velocities $U_a < 0.4$ m/s, the surface roughness effect on the drag force appears to be negligible for all non-serrated leaves of the rigidities R1 and R3. However, at higher velocities, the dependence on the surface roughness becomes noticeable, i.e., the surface roughness increases drag, as one would expect (Figs. 9a, 10a). No significant difference between one-side smooth/one-side rough and two-side rough elliptic and pinnate leaves is observed for these rigidities while two-side rough rectangular leaf experiences higher drag than its two-side smooth and one-side smooth/one-side rough counterparts. The drag coefficient distributions follow a similar tendency as in the drag force plots (Figs. 9b, 10b). No sharp change of the C_d is observed for roughened leaves suggesting that no drag crisis effect occurred within the studied range of Re .

Fig. 9 **a** Plot of the drag force, F , versus the mean approach velocity, U_a , **b** Drag coefficient, C_d , **c** Standard deviation, σ_d , **d** Coefficient of variation, CV , **e** Skewness, S_d , and **f** Kurtosis, K_d of drag force versus Reynolds number, Re ; data for the two side-smooth, one-side smooth/one-side rough and two-side rough smooth edged elliptic, pinnate and rectangular leaves of rigidity R1 are shown

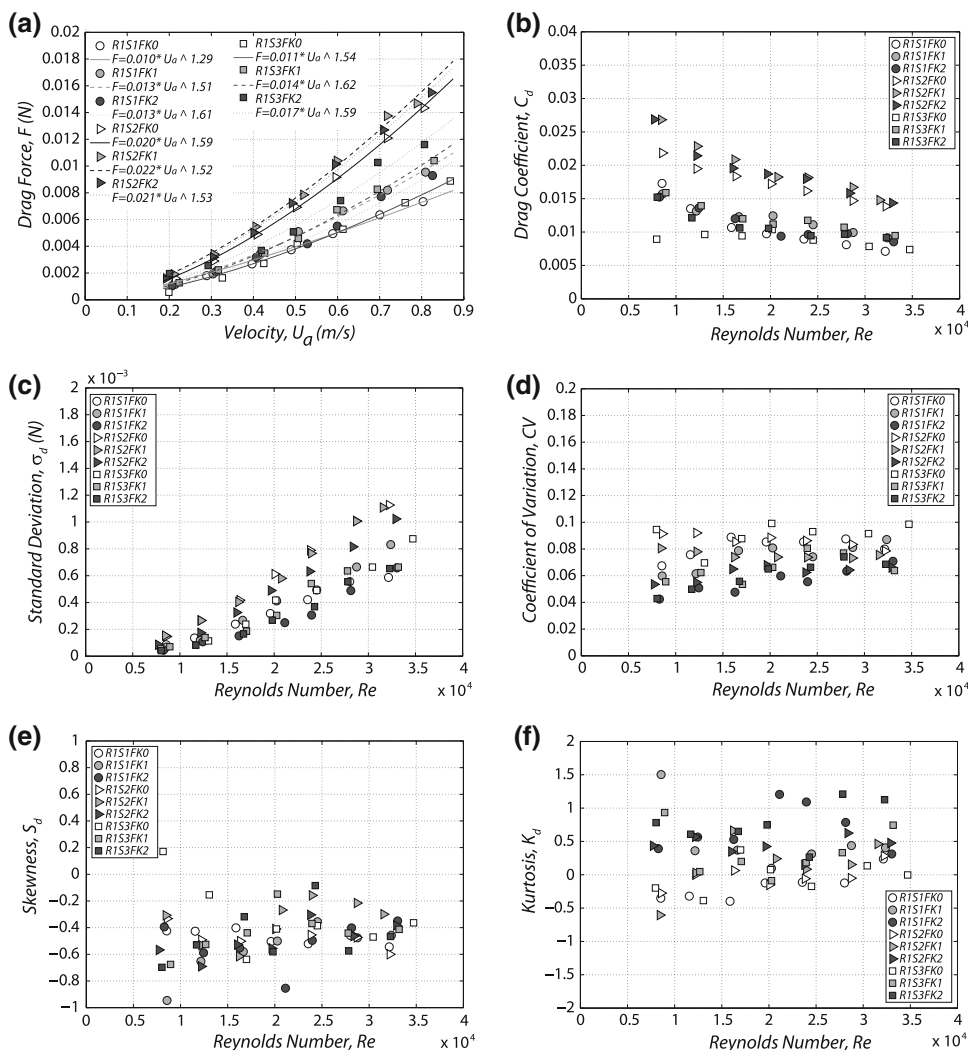
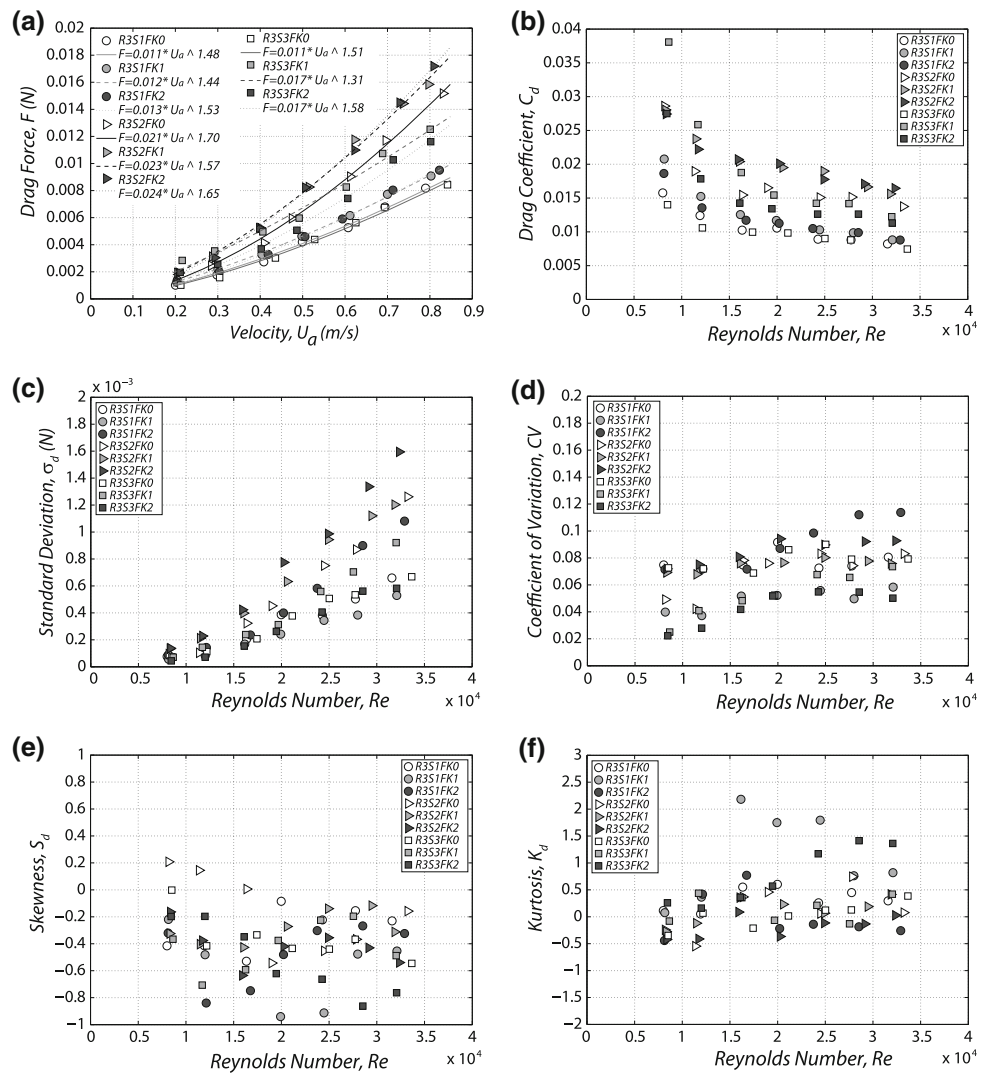


Fig. 10 **a** Plot of the drag force, F , versus the mean approach velocity, U_a , **b** Drag coefficient, C_d , **c** Standard deviation, σ_d , **d** Coefficient of variation, CV , **e** Skewness, S_d , and **f** Kurtosis, K_d of drag force versus Reynolds number, Re ; data for the two side-smooth, one-side smooth/one-side rough and two-side rough smooth edged elliptic, pinnate and rectangular leaves of rigidity R3 are shown



At the highest rigidity R5, the differences in the drag force between smooth and rough leaves tend to increase with increasing velocity (Fig. 11a). Particularly, the surface roughness strongly increases the drag force for the elliptic leaf, whereas its effect on the drag force for the rigid pinnate and rectangular leaves is noticeably lower. The pinnate and elliptic leaves at R5 experience steady increase in the drag force from the two-side smooth to one-side smooth/one-side rough to two-side rough leaves. In contrast, no significant difference between one-side smooth/one-side rough and two-side rough rectangular leaves is observed. The drag coefficients of one-side smooth/one-side rough and two-side rough rectangular and elliptic leaves are approximately constant, being 50% higher than the C_d of their two-side smooth counterparts (Fig. 11b). For this rigidity, a considerable decrease of the drag coefficient is observed for the pinnate leaf until Re reaches 20×10^3 and then the curve $C_d = f(Re)$ becomes flat at higher Re . Also, the drag coefficient of the two-side

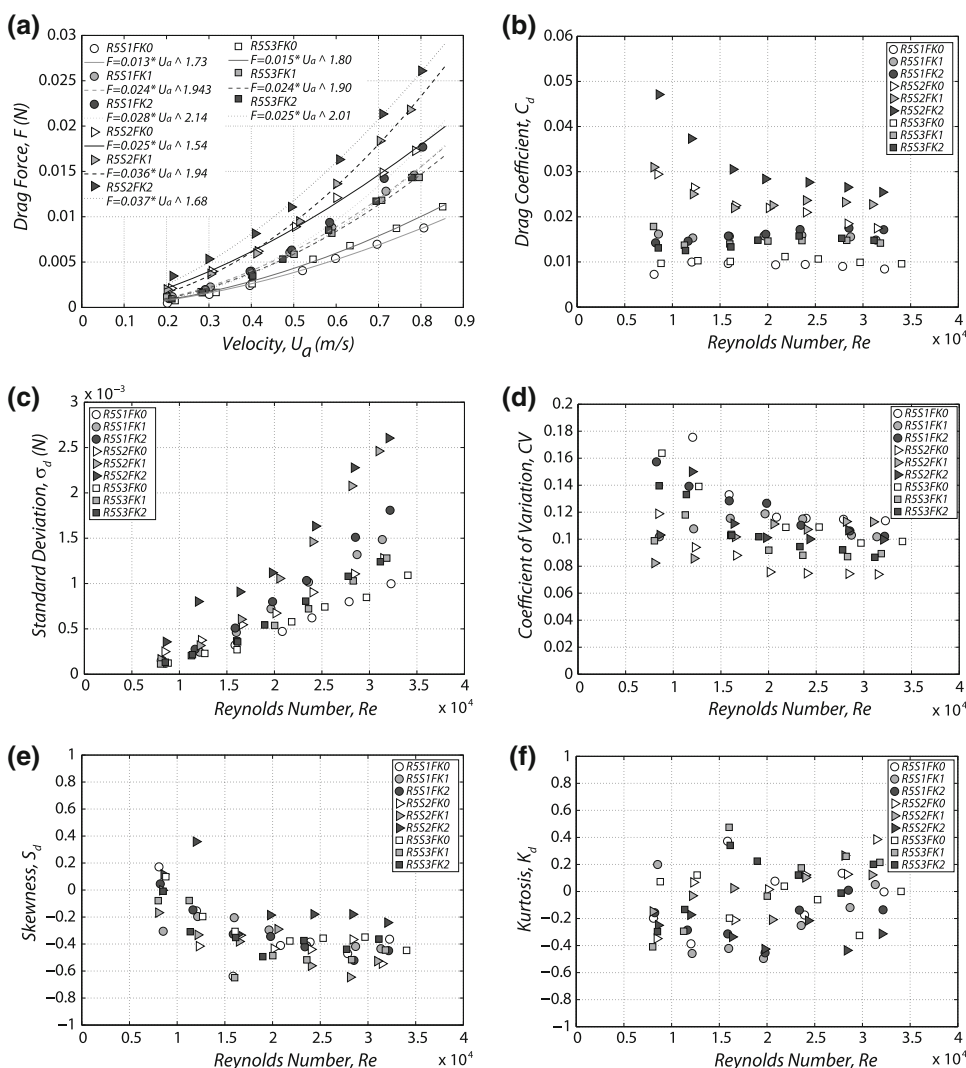
rough pinnate leaf is much higher than the drag coefficients of the two-side smooth pinnate leaf within whole range of Re .

The magnitude of the drag fluctuations quantified with σ_d is shown in Figs. 9c, 10c, and 11c as a function of Re for three rigidities. A strong effect of the roughness on σ_d with a 100% increase at the maximum velocity is clearly seen for the rigid leaves. This is reflected in the distribution of CV of the drag force (Fig. 11d). The effect of surface roughness on the skewness and kurtosis (Figs. 9e, f, 10e, f, 11e, f) is not profound, i.e., the plots of S_d and K_d are similar to those already described based on Figs. 6, 7, and 8.

Effect of roughness on the performance of serrated leaves

The drag force, its statistics and the drag coefficient results for the serrated smooth and rough leaves are shown in

Fig. 11 **a** Plot of the drag force, F versus the mean approach velocity, U_a , **b** Drag coefficient, C_d , **c** Standard deviation, σ_d , **d** Coefficient of variation, CV , **e** Skewness, S_d , and **f** Kurtosis, K_d of drag force versus Reynolds number, Re ; data for the two side-smooth, one-side smooth/one-side rough and two-side rough smooth edged elliptic, pinnate and rectangular leaves of rigidity R5 are shown

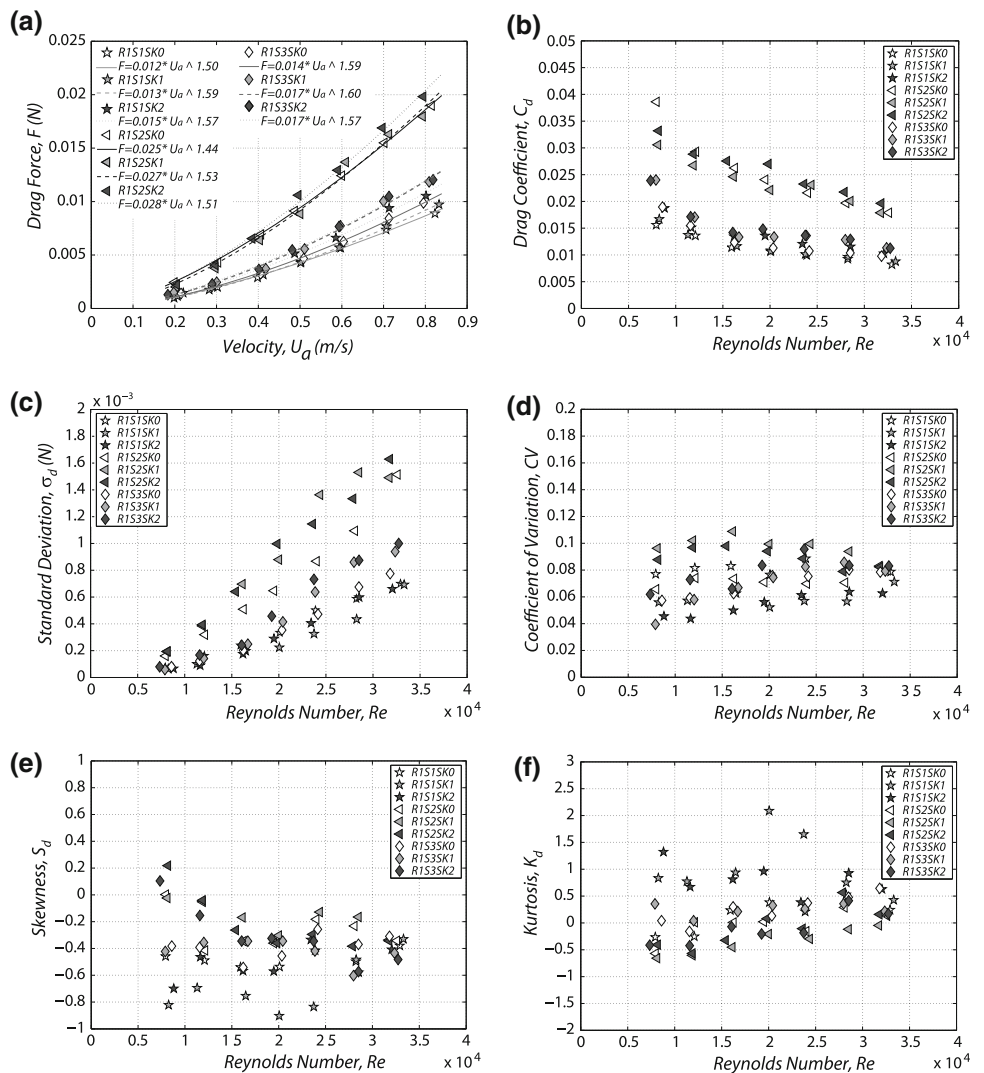


Figs. 12, 13 and 14. These figures show two different behaviors of the drag force distribution versus the mean approach velocity. Firstly, the roughness does not affect the mean drag force of all leaf shapes for velocities $U_a < 0.4$ m/s, independently of the rigidity. However, with increasing velocities, the drag force for the rough leaves becomes higher than that for two-side smooth leaves. The difference between them depends on the rigidity of the leaves: it increases with rigidity (Figs. 12a, 13a, 14a). The difference in the drag force between the one-side smooth/one-side rough and two-side rough leaves is almost negligible for the serrated pinnate and rectangular leaves, whereas a noticeable difference is seen between one-side smooth/one-side rough and two-side rough serrated elliptic leaves. For the low and medium rigidity, R1 and R3, the curves $C_d = f(Re)$ for different leaf shapes are well separated within the whole range of Re , with the highest C_d for the pinnate leaf and the lowest C_d for the elliptic and rectangular leaves (Figs. 12b, 13b). For all shapes, the drag

coefficient decreases with increase in Re up to its maximum studied value, with the roughness effect becoming visible at higher Re . On the other hand, the C_d of the rigid two-side rough serrated leaves (R5) does not change within the whole range of Re , being almost constant (Fig. 14b). Comparing Fig. 11b with Fig. 14b, one may note that the serration serves as a significant drag-enhancing mechanism. In combination with the near-quadratic relationship between the velocity and drag force (Fig. 14a, b) suggests that the serration, roughness and high rigidity of the leaves prevent leaf reconfiguration in the flow that could control and reduce the drag force. As far as the drag crisis is concerned, there is no sharp decline of the C_d in the studied range of Re for the rough serrated leaves.

Similar to the rough non-serrated leaves, the roughness strongly affects the σ_d of the serrated leaves for all rigidities, especially at higher Re (Figs. 12c, 13c, 14c). Interestingly, the drag force variability (CV) of the rough serrated elliptic leaf at rigidity R5 is similar to the CV of

Fig. 12 **a** Plot of the drag force, F versus the mean approach velocity, U_a , **b** Drag coefficient, C_d , **c** Standard deviation, σ_d , **d** Coefficient of variation, CV , **e** Skewness, S_d , and **f** Kurtosis, K_d of drag force versus Reynolds number, Re ; data for the two side-smooth, one-side smooth/one-side rough and two-side rough serrated elliptic, pinnate and rectangular leaves of rigidity R1 are shown



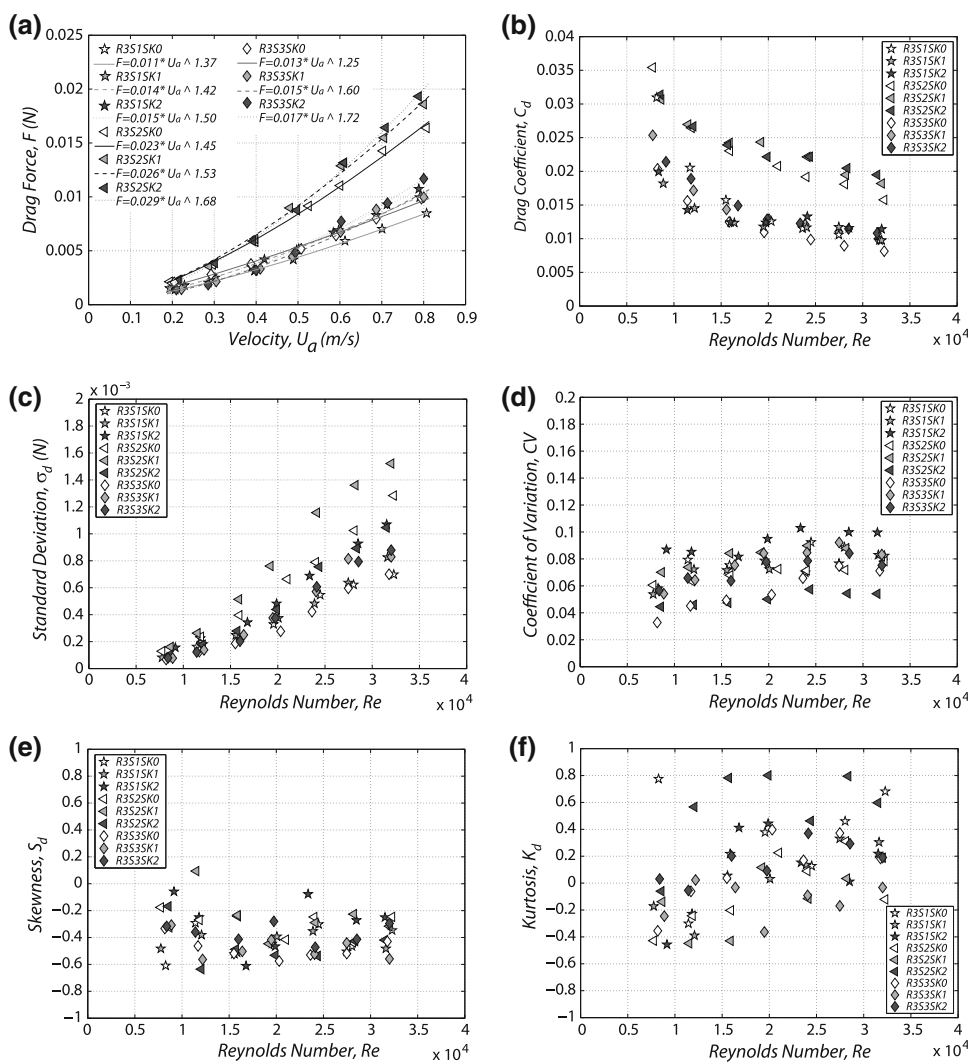
the non-serrated elliptic leaf being higher than other two leaves at higher Re (Fig. 14d). The roughness has a minor effect on the S_d in the whole range of Re independently of the rigidity, with S_d decreasing from 0 at low Re to -0.6 at high Re (Figs. 12e, 13e, 14e), as for the cases of smooth-edge leaves. As for the kurtosis, the situation is similar: no significant effect of serration can be observed (Figs. 12f, 13f, 14f).

Effect of rigidity

Compared to the leaf shape, serration and roughness, the flexural rigidity has a different hydrodynamic effect on leaf behavior in the flow. If the leaf shape, serration and roughness generate a variety of mechanisms of skin friction and determine the surrounding flow patterns, the flexural rigidity may significantly modify these mechanisms and patterns by allowing the leaves to be ‘statically’ re-shaped

(static reconfiguration) as well as to be engaged in dynamic interactions with the flow (dynamic reconfiguration). The magnitude of this effect depends on the Young’s modulus and second moment of area of leaves. From the image analysis and force measurements, we observed that the leaves with rigidity R3 performed similar to the leaves with rigidity R1. The drag forces acting on the leaves with rigidity R1 were lower and scaled quasi-linearly with the velocity, similar to a flexible body in the flow for $Re > 15 \times 10^3$ (Vogel 1994). The Vogel number (α) ranged between -0.7 and -0.5 . Lower rigidity allowed the leaves to undulate and streamline in the flow to reduce the overall drag force as can be clearly seen by comparing Figs. 6b to 14b. For the highest rigidity (R5), the leaves experienced noticeably higher drag forces than those with lower rigidities. For this case, the drag force was a function of squared velocity while the drag coefficients were quasi-constant (i.e., largely independent on Re).

Fig. 13 **a** Plot of the drag force, F versus the mean approach velocity, U_a , **b** Drag coefficient, C_d , **c** Standard deviation, σ_d , **d** Coefficient of variation, CV , **e** Skewness, S_d , and **f** Kurtosis, K_d of drag force versus Reynolds number, Re ; data for the two side-smooth, one-side smooth/one-side rough and two-side rough serrated elliptic, pinnate and rectangular leaves of rigidity R3 are shown



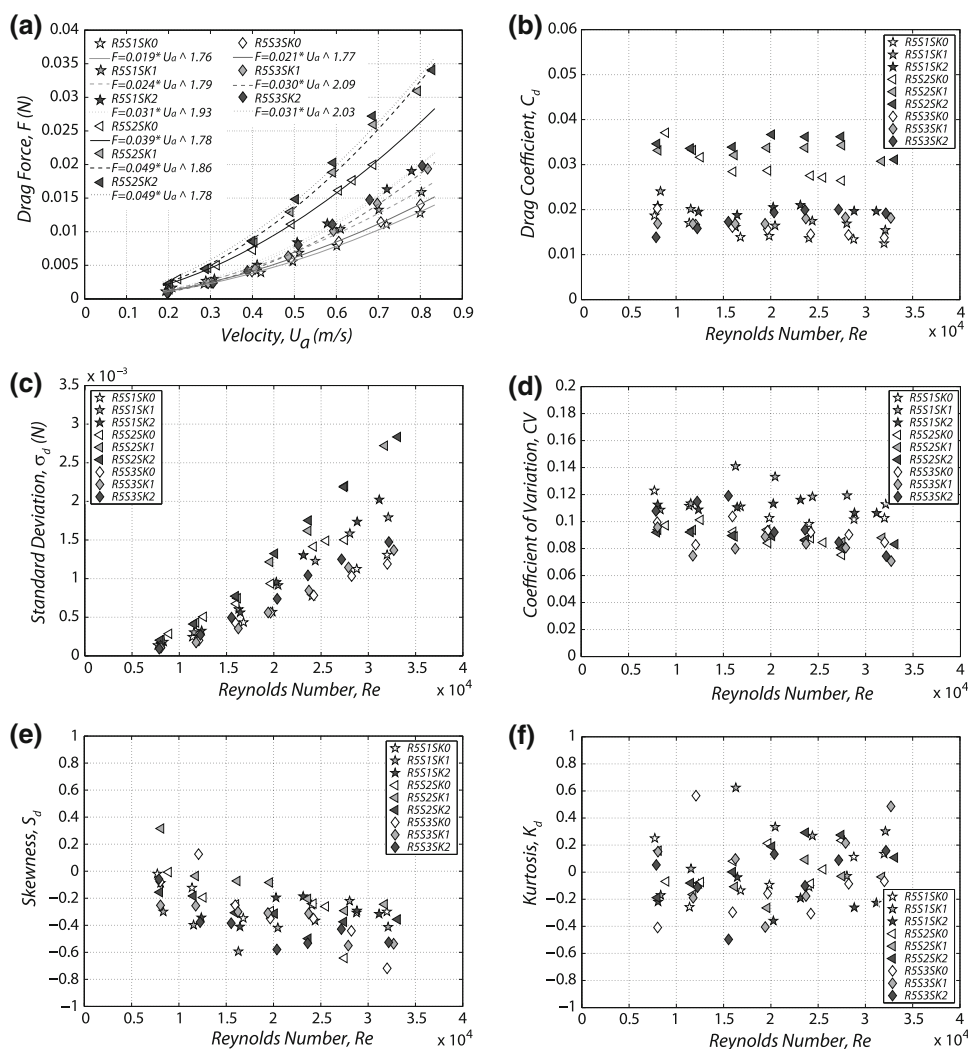
Turbulence effect on drag force statistics

The plot of the standard deviation of the approach velocity σ_{U_a} versus the standard deviation of the drag force σ_d for all leaf configurations is shown in Figs. 15a–c for the rigidities R1, R3 and R5, respectively. There are clear relationships of the σ_d with the turbulence levels showing two different tendencies (Fig. 15). At small values of $\sigma_{U_a} < 0.025$ m/s the effect of ambient turbulence on the σ_d is not significantly influenced by the leaf properties (shape, serration, roughness and rigidity) and the drag standard deviation is fairly linearly proportional to the standard deviation of the instantaneous streamwise velocity. However, at a higher level of velocity fluctuations ($\sigma_{U_a} > 0.025$ m/s), the strength of the effects of the leaf properties on the relationship between the σ_{U_a} and the σ_d significantly increases. Comparing Fig. 15a–c, one can note that for all three shapes the drag standard deviation σ_d at the same σ_{U_a} considerably increases from relatively low values at R1 to the high values at R5, reflecting the diminishing effect of dynamic reconfiguration on the leaf

performance with increase in rigidity. The shape also strongly affects the relations between velocity and drag fluctuations, with a pinnate shape being the most efficient in enhancing effects of turbulent fluctuations on the drag force variability. Plots in Fig. 15 suggest that there is a threshold value of $\sigma_{U_a} = 0.025$ m/s that separates two leaf-flow interaction regimes: (I) passive interaction at $\sigma_{U_a} < 0.025$ m/s; and (II) active interaction at $\sigma_{U_a} > 0.025$ m/s.

Figures 16a and b show the skewness (S_d) and kurtosis (K_d) of the drag force versus the skewness (S_{U_a}) and kurtosis (K_{U_a}) of the approach velocity for all leaf configurations, respectively. The values of the S_d are mainly negative, up to -1.0 , with values of the S_{U_a} staying in the range from -0.1 to -0.5 (Fig. 16a). This result indicates that the negativity in the S_d is likely imposed by turbulence. The values of the K_d change mostly between -0.5 and 0.75 (with few outliers) while the K_{U_a} varies between -0.2 and 0.5 . A general positive trend between K_d and the K_{U_a} can be clearly seen in Fig. 16b. Negative kurtosis indicates that the probability distributions have a

Fig. 14 **a** Plot of the drag force, F versus the mean approach velocity, U_a , **b** Drag coefficient, C_d , **c** Standard deviation, σ_d , **d** Coefficient of variation, CV , **e** Skewness, S_d , and **f** Kurtosis, K_d of drag force versus Reynolds number, Re ; data for the two side-smooth, one-side smooth/one-side rough and two-side rough serrated elliptic, pinnate and rectangular leaves of rigidity R5 are shown



wider peak around the mean and thinner tails while positive kurtosis shows a sharper peak around the mean reflecting an increased intermittency compared to the normal distribution. Figure 16b shows that the range of K_d is appreciably higher than that for the velocity, reflecting higher intermittency in drag force fluctuations. This higher intermittency is probably due to the non-linear responses of the leaves to the flow. It should be also noted that leaf properties affect the wake turbulence intensity. The serrated leaves clearly enhance the wake turbulence while non-serrated leaves for all rigidities and shapes either don't modify or surpass it, especially for the rough leaves. However, it should be stressed that this finding is based on only single point velocity measurements at 5 cm downstream of the back tip of a leaf.

Discussion

This investigation is the first systematic study of flow-plant interactions at the leaf scale, providing important insights

into the effects of the leaf properties on the drag forces experienced by leaves in flowing water.

In freshwater, both light and carbon are more difficult to attain for plants than in terrestrial ecosystems. Hence, strong selection pressures can be expected to optimize plant morphology for light and carbon capture (Madsen and Sand-Jensen 2006). Leaves are the major photosynthetic organs of plants and, with respect to photosynthetic performance, three major requirements dictate the basic shape and form of a leaf. A wide surface area allows for the capture of light energy, a low thickness provides efficient gas-exchange and a means to transport the products of photosynthesis to plant tissues (Scott 2008). In addition, leaves are reconfiguring in moving fluids (terrestrial leaves in air, aquatic leaves in water) and hence photosynthetic activity and leaf reconfiguration for drag control are balanced and traded off with each other. Thus, shape, serration, surface roughness and flexural rigidity of leaves, varying widely across different plants, are likely to be optimized by plants to adapt to their habitats. Therefore,

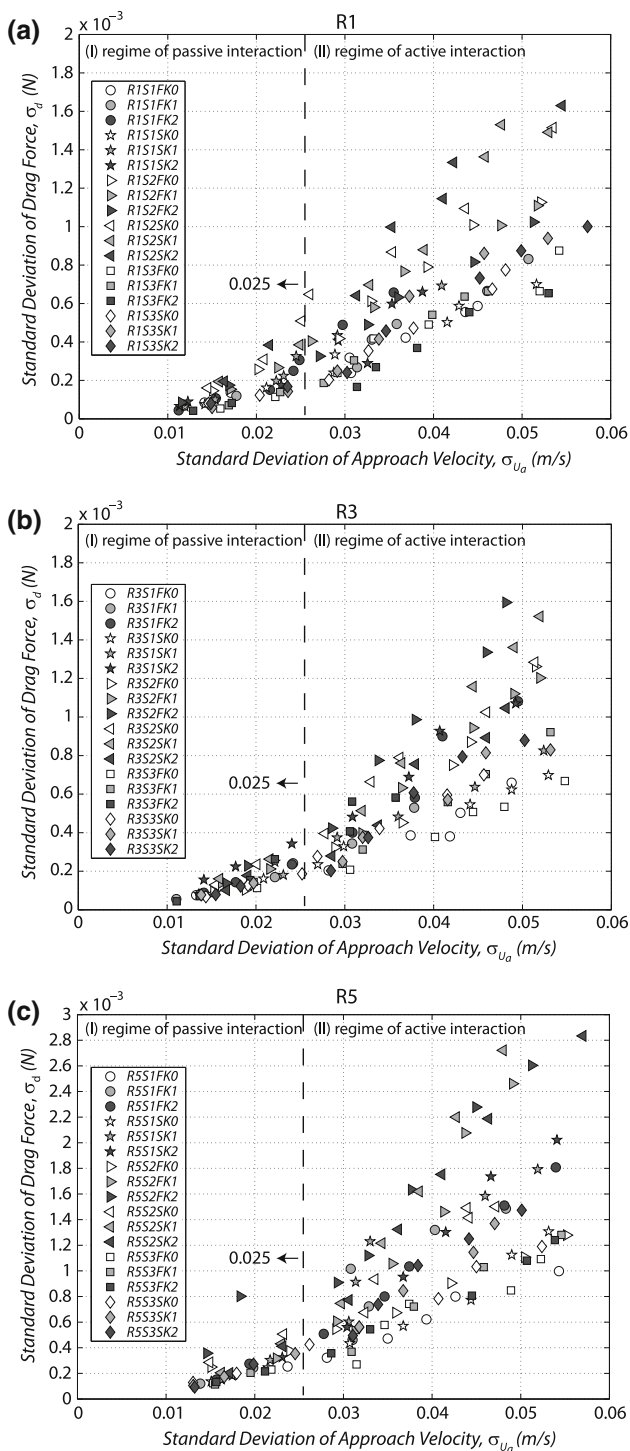


Fig. 15 Plot of the drag force standard deviation, σ_d versus the standard deviation of the approach velocity, σ_{U_a} for all leaf configuration of the rigidity R1 (a), R3 (b) and R5 (c)

many possible leaf configurations were considered in this investigation. The artificial leaves we used in this study were similar to natural leaves in shape, serration, roughness and flexural rigidity. The pinnate, rectangular and elliptic leaves broadly resemble the leaves of aquatic plant species,

e.g. *Myriophyllum alterniflorum* (pinnate shape), *Glyceria fluitans* (rectangular, strap-like shape) and *Elodea canadensis* (elliptic shape).

The flexural rigidity of *G. fluitans* leaves is $8...38 \times 10^{-8} \text{ Nm}^2$ i.e., of the same order of magnitude as R1. *G. fluitans* prefer to live in a habitat of slow to moderate flowing water. The experimental results presented here for the flexible, one-side rough artificial rectangular leaf with a smooth margin showed its good performance (i.e., less drag) for velocities less than 0.5 m/s compared to the other leaf configurations. In this case, reconfiguration is dominated by the small deflection of the leaf and the parallel alignment to the flow causes the leaf to be loaded in tension. Hence, this results in an overall reduced drag force, drag standard deviation and coefficient of variation, and a decline in the drag coefficient (Fig. 6a–d). At flow velocities larger than 0.5 m/s, dynamic reconfiguration of the leaf occurs, i.e. the leaf changes its shape by undulating and/or reducing the frontal area which might reduce the drag force acting on it. This can be seen in the negative skewness and the positive kurtosis of the drag force at high Re, indicating that the leaf fluctuations generate frequent positive (but small) and rare negative (but deep) variations of the instantaneous drag force. A similar mechanism was observed for the flexible elliptic leaf. The leaves of *G. fluitans* have a strap-like shape similar to the rectangular leaf, but may show a better hydrodynamic performance due to their surface texture, which consists of linear ridges that are aligned parallel to the flow direction.

When exposed to the load of a fluid flow, the pinnate leaf experienced higher drag force, standard deviation and drag coefficient than the other leaves due to its complex geometry with 12 leaflets and a larger perimeter, width, and frontal area. Flow separations from the leaflets of the pinnate leaf creates a variety of instabilities preventing reconfiguration of the pinnate leaf such as folding and streamlining in order to reduce the drag imposed by flow. However, the drag force variability (CV) was nearly constant and equal for three leaf shapes at high Re implying that the leaf geometry does not strongly affect the CV, which is likely controlled by the ambient turbulence characteristics. With increase in rigidity and adding the serration and roughness to the pinnate leaf, the drag force, standard deviation and the drag coefficient were almost doubled in the experiments, resulting in a decline of performance (i.e., increase in drag). The different configurations of the pinnate leaf presented here simulate natural plant leaves that are commonly found in aquatic and terrestrial plants, e.g. *Ranunculus penicillatus* and *Ranunculus sceleratus*, respectively (Fig. 17). Often aquatic plants have extremely flexible and finely dissected leaves, e.g. *R. penicillatus* and *M. alterniflorum*. Dissected leaves have a higher surface area to volume ratio than

Fig. 16 **a** Drag force skewness, S_d versus the skewness of the approach velocity, S_{Ua} for all leaf configurations and rigidities together, and **b** the kurtosis of the drag force, K_d versus the kurtosis of the approach velocity, K_{Ua} for all leaf configurations and rigidities together

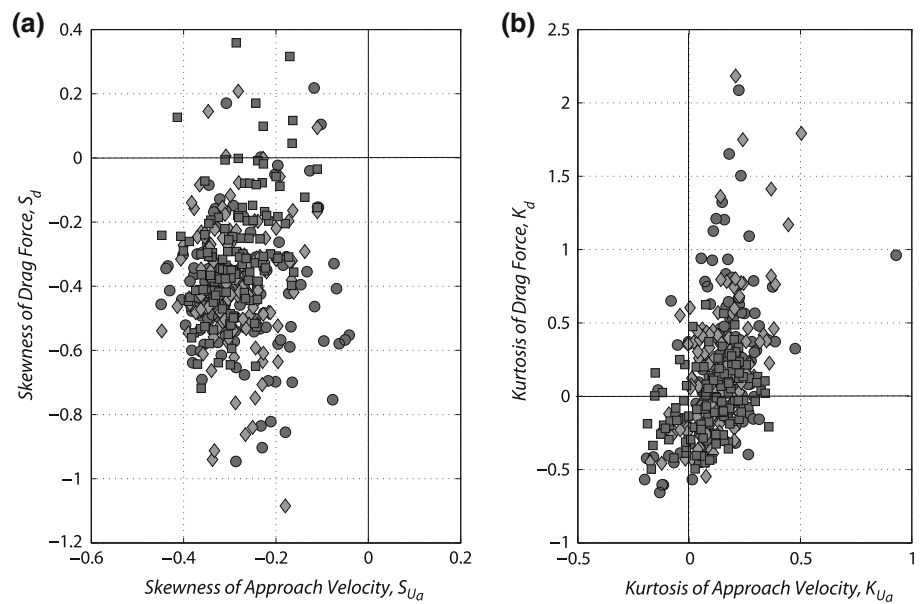
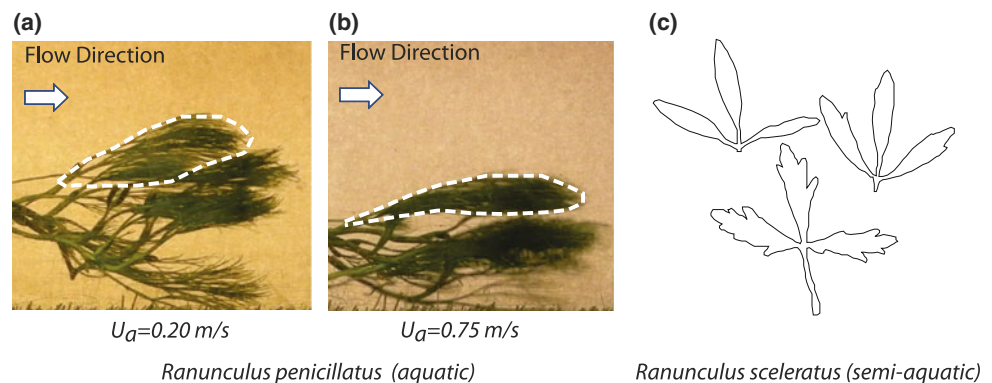


Fig. 17 Video images captured from force and velocity experiments that were performed with *R. penicillatus* at $U_a = 0.2$ m/s **(a)** and 0.75 m/s **(b)** in the laboratory of the University of Aberdeen and a sketch of the leaves of *R. sceleratus* **(c)**



aerial leaves and they offer less mechanical resistance to the flow (Sculthorpe 1967). This is due to the lack of a stiffening cuticula in submerged aquatic plant leaves (Niklas and Paulillo 1997). Figure 17a, b show a good example of the reconfiguration of *R. penicillatus* with increasing velocity: at higher flow rates, the leaves become largely compressed and their leaflets are adopting a more streamlined elliptic shape, which is similar to the artificial elliptic leaf in our study. A similar folding of the single leaflets towards the central leaf axis has been observed for the leaves of many palm species (Niklas 1999). The experiments confirmed that the elliptic leaf had a better hydrodynamic shape than the other leaves at higher flow rates as it experiences less drag force due to its streamlined shape and smaller frontal area. In this way, the leaf shape becomes hydrodynamically advantageous to tolerate the drag force imposed by the flow and these structural and hydrodynamic features of dissected leaves possibly enhance the ability of these species to adapt to high flow velocities and colonize even fast flowing rivers.

Although serration is not common for submerged plant leaves, several species have serrated leaves. For example, *E. densa*, *H. verticillata* and *Potamogeton crispus* have elongated elliptic leaves with prominent teeth along the leaf margins. They primarily inhabit lakes. Our experiments showed that serration did not largely increase the mean drag force but enhanced the turbulence intensity around the leaf at lower Reynolds numbers. For plant growth and photosynthesis, gas exchange between leaf surface and the water column is important and thus, turbulence enhancement due to serration strongly influences gas exchange for aquatic plants living in lakes and slow-flowing rivers. In a similar way, Gottschlich and Smith (1982) proposed that serration increases turbulence intensity, and thus increases convective heat loss at low Reynolds numbers on modeled elliptic terrestrial leaves with differently serrated margins. On the other hand, in fast-flowing streams, the serration causes high drag forces acting on the leaf. Since turbulence is already high in these flow conditions, river plants are unlikely to have leaves with toothed margins.

The effect of surface roughness on drag force can have opposite trends. When the surface roughness is high relative to the thickness of the viscous sublayer, protruding rough elements on a leaf surface can cause a considerable increase in the drag force. Our results clearly confirmed this trend for the rough leaves. On the other hand, one may also observe drag reduction when the surface roughness is comparable to the thickness of the viscous sublayer. It should be also noted that surface roughness patterns may play an important role in the drag reduction and may increase or decrease the drag force. For example, aquatic *G. fluitans* leaves have a smooth bottom side and a rough upper side with sawtooth-like riblets that are triangular in cross-section and aligned in a streamwise direction. Such a ribbled surface has been shown to reduce turbulence skin friction and hence results in a 5% drag reduction in turbulence flow (Tani 1988; Bechert et al. 1997). We suggest that the rectangular leaves with such a surface roughness pattern should have a better hydrodynamic performance than the smooth rectangular leaves used in our experiments. The hydrodynamic performance furthermore depends on the flexural rigidity of the leaves, with flexible leaves experiencing a reduced drag force compared to rigid leaves.

The turbulence effects on the drag statistics were analyzed and a strong relationship was found between the ambient turbulence and the drag force statistics. Our data highlighted two regimes of flow-leaf interaction separated by a threshold value of the ambient turbulence level. In the first regime (passive interaction), as shown in Fig. 15, the drag statistics are controlled by the turbulence statistics at low turbulence levels. On the other hand, in the second regime (active interaction) the effects of the leaf properties on the drag statistics become significant and comparable to the turbulence contribution at high turbulence levels. The ambient turbulence also affects the distributions of the third and fourth moments of the drag force (S_d and K_d). The negativity in the skewness and intermittency in the instantaneous drag force are likely imposed by turbulence. The noted increased values of the kurtosis of the fluctuating drag force, which exceed those for velocity, is most likely due to the non-linear interactions between leaves and flow. Thus, the imprint of turbulent flow can clearly be found in the drag force statistics.

Conclusion

Our study demonstrated that the effects of all four leaf parameters are strongly interconnected in respect to drag control/reduction. The results show that the leaf shape is the most important factor determining hydrodynamic interactions, with flexural rigidity, serration and roughness

changing only the magnitude but not the direction of the effect on drag control. For the reconfiguration of the leaves, flexural rigidity is the most influential parameter. The serration effect is highly dependent on the flexural rigidity since only very rigid leaves show a strong effect of serration. Serration furthermore changes the turbulence pattern around the leaves by increasing the downstream turbulence intensity. One-side and two-side roughness both were observed to enhance the drag force acting on the leaf at high Reynolds numbers. In addition, two-side roughness together with serration doubles the drag force on a leaf. It is likely that the habitat flow characteristics together with other environmental factors such as light intensity, temperature and nutrient availability determine the morphological and biomechanical traits of plant leaves, which optimize the relative importance of shape, rigidity, serration and roughness.

Acknowledgments The work was supported by the Leverhulme Trust, Grant F/00152/Z ‘Biophysics of flow-plant interactions in aquatic systems’. The Centre for Ecology & Hydrology (CEH, Edinburgh) supplied the strain gauge equipment used in this work. The authors are grateful to Giulia Pagello and Fabio Siniscalchi for their help with the experimental work.

References

- Armanini A, Righetti M, Grisenti P (2005) Direct measurement of vegetation resistance in prototype scale. *J Hydraul Res* 43:481–487
- Bechert DW, Bruse M, Hage W, Van der Hoeven JGT, Hoppe G (1997) Experiment on drag-reducing surfaces and their optimization with an adjustable geometry. *J Fluid Mech* 338:59–87
- Chen JM, Ibbetson A, Milford JR (1988) Boundary-layer resistances of artificial leaves in turbulent air: I. leaves inclined to the mean flow. *Bound Lay Meteorol* 45:371–390
- de Langre E (2008) Effects of wind on plants. *Annu Rev Fluid Mech* 40:141–168
- Ennos AR (1999) The aerodynamics and hydrodynamics of plants. *J Exp Biol* 202:3281–3284
- Ennos R, Sheffield E (2000) *Plant Life*. Blackwell, London
- Goring D, Nikora V (2002) De-spiking ADV data. *J Hydraul Eng ASCE* 128:117–126
- Gottschlich DE, Smith AP (1982) Convective heat transfer characteristics of toothed leaves. *Oecologia* 53:418–420
- Järvelä J (2002) Flow resistance of flexible and stiff vegetation: a flume study with natural plants. *J Hydrol* 269(1–2):44–54
- Koch K, Bhushan B, Barthlott W (2009) Multifunctional surface structures of plants: an inspiration for biomimetics. Invited Review. *Prog Mater Sci* 54:137–178
- Madsen TV, Sand-Jensen K (2006) Aquatic Plants. In: Running waters: historical development and restoration of lowland Danish streams. In: Sand-Jensen K (ed); Nikolai Friberg; John Murphy National Environmental Research Institut: Det Naturvidenskabelige Fakultet, Aarhus Universitet, pp 67–74
- Miler O, Albayrak I, Nikora V, O’Hare M (2011) Biomechanical properties of aquatic plants and their effects on plant-flow interactions in streams and rivers. *Aquat Sci*. doi:10.1007/s00027-011-0188-5
- Niklas KJ (1999) Research review: a mechanical perspective on foliate leaf form and function. *New Phytol* 143:19–31

- Niklas KJ, Paolillo DJ (1997) The role of the epidermis as a stiffening agent in *Tulipa* (Liliaceae) stems. *Am J Bot* 84:734–744
- Nikora V (2010) Hydrodynamics of aquatic ecosystems: an interface between ecology, biomechanics and environmental fluid mechanics. *River Res Appl* 26:367–384
- Nikora V, Goring DG (1998) ADV measurements of turbulence: can we improve their interpretation? *J Hydraul Eng ASCE* 124:630–634
- O'Hare MT, Clarke RT, Bowes MJ, Cailes C, Henvile P, Bissett N, McGahey C, Neal M (2010) Eutrophication impacts on a river macrophyte. *Aquat Bot* 92:173–178
- Preston C D, Croft J M (2001) *Aquatic Plants in Britain and Ireland*. Harley Books
- Riemer DN (1993) *Introduction to freshwater vegetation*. Krieger Publishing Company, Melbourne, Florida, reprint. 1-800-724-0025
- Sand-Jensen K (2003) Drag and reconfiguration of freshwater macrophytes. *Freshwater Biol* 48:271–283
- Schouveiler L, Boudaoud A (2006) The rolling up of sheets in a steady flow. *J Fluid Mech* 563:71–80
- Schuepp PH (1993) Leaf boundary layers: Tansley Review No. 59. *New Phytol* 125:477–507
- Scott P (2008) *Physiology and behaviour of plants*. Wiley, Chichester
- Sculthorpe CD (1967) *The biology of aquatic vascular plants*. Edward Arnold, London, p 610
- Statzner B, Lamouroux N, Nikora V, Sagnes P (2006) The debate about drag and reconfiguration of freshwater macrophytes: comparing results obtained by three recently discussed approaches. *Freshwater Biol* 51:2173–2183
- Tani I (1988) Drag reduction by riblet viewed as a roughness problem. *Proc Jpn Acad B* 64:21–24
- Tsukaya H (2005) Leaf shape: genetic controls and environmental factors. *Int J Dev Biol* 49:547–555
- Usherwood JR, Ennos AR, Ball DJ (1997) Mechanical adaptations in terrestrial and aquatic buttercups to their respective environments. *J Exp Bot* 48:1469–1475
- Vogel S (1989) Drag and reconfiguration of broad leaves in high winds. *J Exp Bot* 40:941–948
- Vogel S (1994) *Life in Moving Fluids*, 2nd edn. Princeton University Press, Princeton
- Vogel S (2009) Leaves in the lowest and highest winds: temperature, force and shape. *New Phytol* 183:13–26
- Wilson CAME, Stoesser T, Bates PD, Batemann Pinzen A (2003) Open channel flow through different forms of submerged flexible vegetation. *J Hydraul Eng ASCE* 129:847–853